ARCHIVES OF MECHANICS
Arch. Mech. **77** (3), 305–332, 2025, https://doi.org/10.24423/aom.4650

Influence of rotation and couple stresses on convective stability in Navier–Stokes–Voigt fluid

D. KUMAR[1,*], SUNIL[1], R. DEVI[2]

[1] *Department of Mathematics and Scientific Computing, National Institute of Technology Hamirpur, Hamirpur, 177005, H.P., India, e-mail*[*]*: depk471999@gmail.com (corresponding author)*

[2] *Department of Mathematics, Government College Nagrota Bagwan, Kangra, 176047, H.P., India*

This study investigates the influence of rotation and couple stresses on the convective stability of the Navier–Stokes–Voigt fluid under various boundary conditions, employing both nonlinear (via the energy method) and linear (using the normal mode analysis method) approaches. The eigenvalue problem is derived for both analyses and solved using the Galerkin method to obtain the Rayleigh number. It has been observed that the critical Rayleigh number is identical for both analyses, confirming global stability and the absence of subcritical instabilities. Notably, we find that increasing the couple stress parameter significantly narrows the spectrum of wave numbers for oscillatory modes. Conversely, higher Taylor numbers and Kelvin–Voigt parameters expand the wave number spectrum for oscillatory convection. While couple stresses and rotational effects provide stabilizing influences, the Kelvin–Voigt parameter acts as a destabilizing factor for oscillatory convection. These findings offer valuable insights with potential applications in improving fluid stability and thermal management across a wide array of industries, including industrial cooling systems, aerospace engineering, biomedical devices, energy systems, and environmental engineering.

Key words: nonlinear and linear analyses, couple stresses, rotation, Navier–Stokes–Voigt fluid.

1. Introduction

Thermal convection in viscoelastic fluids is a fundamental area of study in fluid mechanics, with significant implications across various scientific and engineering fields. Unlike Newtonian fluids, viscoelastic fluids exhibit both viscous and elastic properties, resulting in complex flow behavior. When thermal gradients come into play, this complexity becomes particularly important for understanding the onset of instabilities and the transition to convective motion. In this context, external factors such as rotation play a role, while stresses, which are internal forces that arise due to the material's response to these external influ-

ences, contribute to the development of these instabilities. CHANDRASEKHAR [1] extensively reviewed theoretical and experimental insights into thermal instability, focusing on the Bénard convection in fluid layers. JOSEPH [2] examined fluid rheology and various models for viscoelastic fluids. STRAUGHAN [3] presented constitutive equations for the Maxwell, Oldroyd, and Kelvin–Voigt models, highlighting the sensitivity of solutions to viscoelastic coefficients and parameters in boundary-initial value problems for the first-order Kelvin–Voigt fluids. The Kelvin–Voigt model effectively represents linear viscoelastic behavior under small deformations [4]. ZVYAGIN and TURBIN [5] described the Kelvin–Voigt model as a parallel combination of viscosity and elasticity, further classifying it into distinct orders. The zeroth-order Kelvin–Voigt fluid, known as the Navier–Stokes–Voigt (NSV) fluid [6], characterizes materials with weak viscoelastic properties. Recent investigations into thermal convection in NSV fluids, including those by STRAUGHAN [7, 8], BADDAY and HARFASH [9], BASAVARAJAPPA and BHATTA [10], KAVITHA *et al.* [11], AFLUK and HARFASH [12], and SHARMA *et al.* [13], have advanced our understanding of this fluid's behavior under various effects.

Couple stresses, a concept used to describe some non-Newtonian fluids, arise from internal rotational interactions, adding extra stress components to the traditional viscous stresses. These stresses result from microscopic effects, such as particle rotation or fluid deformation, and can be treated as higher-order terms in the stress tensor, similar to the biharmonic plate problem in solids, which accounts for torsional moments. STOKES [14] developed the theory of couple stresses in fluids, highlighting their significance in fluids containing large molecules where these stresses play a crucial role. The influence of couple stresses on the effective viscosity of magnetic fluids has been explored by WENG [15], providing insights into how these stresses modify fluid behavior in magnetic fields. SUNIL *et al.* [16] investigated global stability for thermal convection in couple stress fluids with free-free boundaries, while SUNIL and DEVI [17] examined the same stability in the context of rigid-rigid boundaries. Recent work by AFLUK and HARFASH [18] has explored the stability and instability of thermosolutal convection in the Brinkman–Darcy–Kelvin–Voigt fluid, incorporating the effects of couple stresses. A number of researchers have further investigated the role of couple stresses in fluids, including LIN [19], SHIVAKUMARA and KUMAR [20], SHANKAR *et al.* [21], MAHAJAN and NANDAL [22], CHOUDHARY *et al.* [23], THAKUR *et al.* [24], and AFLUK and HARFASH [25]. These studies highlight the increasing importance of couple-stress effects in fluid dynamics, with implications for industrial applications, material processing, and environmental engineering, offering potential for better designs and more efficient processes.

Rotation refers to the motion of an object or fluid around an axis, significantly influencing the behavior and dynamics of the system. In fluid mechanics, rotation

introduces additional forces, such as the Coriolis force, which alter flow characteristics. This phenomenon is vital in understanding fluid behavior in natural systems like the atmosphere and oceans, as well as in engineering applications such as rotating machinery. One of the key effects of rotation is its stabilizing influence on convection, as demonstrated by GALDI and STRAUGHAN [26] in their study of the Bénard problem. They showed how rotation can lead to more stable convection patterns in fluid systems. The impact of rotation extends to complex systems like convection in porous media. For instance, SHARMA *et al.* [27] explored the thermosolutal instability of Walters' rotating fluid in a porous medium, illustrating how rotation affects fluid behavior under varying thermal and solutal conditions. Similarly, SUNIL *et al.* [28] examined the effects of rotation in the presence of throughflow during Bénard convection in a porous medium, highlighting its role in influencing heat transfer and fluid motion in hydromagnetic systems. MALASHETTY *et al.* [29] studied thermal convection in a rotating viscoelastic fluid saturated porous layer, demonstrating that rotation plays a critical role in heat transfer processes in such environments. More recently, THAKUR *et al.* [30] have analyzed the impact of rotation on ferroconvection in a porous medium with couple stress forces, emphasizing how nonlinear effects and rotation together influence the system's stability and behavior. The importance of rotation in fluid dynamics lies in its ability to modify flow patterns, stabilize or destabilize convection, and significantly impact heat and mass transfer processes. Its role is essential in the analysis and design of various fluid systems, both in natural phenomena and engineered applications.

While many studies have explored the stability of NSV fluids under various effects, the impact of rotation with different boundary conditions is still not fully understood. Previous work by SHARMA *et al.* [13] has investigated some aspects of this topic; however, the influence of couple stresses in the presence of rotation has not been studied yet. In this study, we extend the analysis by investigating the combined impact of both couple stresses and rotation on the stability of NSV fluids, which offers new insights into the interplay between these two factors across various boundary conditions, including rigid-free (where the bottom surface is rigid and the top boundary is free), free-free, and rigid-rigid configurations. Section 2 establishes the governing equations for the system, incorporating perturbation and nondimensionalization to enable analytical progress. In Section 3, nonlinear analysis is performed using the energy method, with the variational principle employed to derive the eigenvalue problem. In Section 4, linear stability analysis is conducted using the normal mode method, leading to the formulation of an eigenvalue problem specific to this approach. Section 5 describes the numerical methods utilized to solve the eigenvalue problems derived in Section 3 and Section 4. Section 6 presents the results and their discussion, including graphical representations that illustrate the influence of key parameters

on the system's stability. The concluding section highlights the key findings and contributions of this study, which, to the best of our knowledge, is a pioneering exploration of these aspects of thermal convection in NSV fluids.

2. Mathematical formulation

Consider an incompressible Navier–Stokes–Voigt fluid layer of infinite length and thickness 'd', subjected to heating from below in the presence of couple stress forces. The system is rotating with an angular velocity $\mathbf{\Omega} = (0, 0, \Omega)$ about the z-axis. The temperature at the lower boundary $z = 0$ is T_o, and at the upper boundary $z = d$, it is T_d, ensuring a uniform temperature gradient $\left(\beta = \left|\frac{dT}{dz}\right|\right)$ across the fluid layer. The force of gravity $\mathbf{g} = -g\hat{\mathbf{k}}$ acts in the negative direction of z-axis, opposing the buoyant forces induced by the temperature difference. The geometric setup is depicted in Fig. 1.

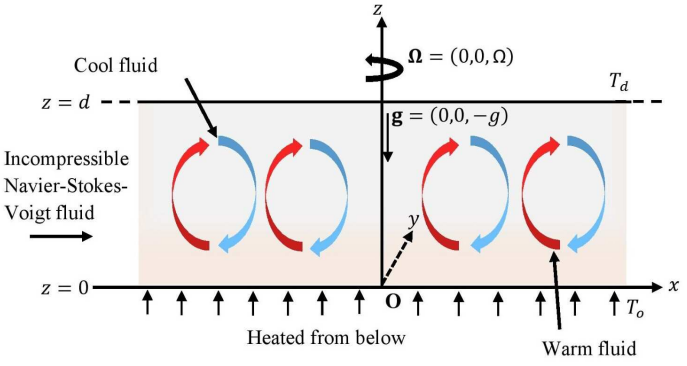

FIG. 1. Geometrical configuration.

The governing equations for the incompressible rotating Navier–Stokes–Voigt fluid system, considering the presence of couple stresses, are as follows [7, 13, 18]:

The equation of continuity

$$\nabla \cdot \mathbf{q} = 0. \tag{2.1}$$

Equations of motion

$$\rho_o\left((1 - \widehat{\lambda}\nabla^2)\frac{\partial}{\partial t} + \mathbf{q}\cdot\nabla\right)\mathbf{q} = -\nabla p + \left(\mu - \mu'\nabla^2\right)\nabla^2\mathbf{q} + \rho_o g\alpha T\hat{\mathbf{k}} + 2\rho_o\left(\mathbf{q}\times\mathbf{\Omega}\right). \tag{2.2}$$

The derivation of the equation of motion for an NSV fluid in the presence of couple stresses is provided in Appendix A.

The energy equation

$$\frac{\partial T}{\partial t} + (\mathbf{q}\cdot\nabla)T = \kappa\nabla^2 T. \tag{2.3}$$

The equation of state

$$\rho = \rho_o\big(1-\alpha(T-T_o)\big). \tag{2.4}$$

Here, we denote the quantities as follows: $\mathbf{q} = (u,v,w)$ for velocity, ρ for density, ρ_o for reference density, p for pressure, $\widehat{\lambda}$ for the Kelvin–Voigt coefficient, μ' for the coefficient of couple stress viscosity, μ for the coefficient of viscosity, t for time, α for the coefficient of thermal expansion, and κ for thermal diffusivity. Also, $\nabla \equiv \left(\frac{\partial}{\partial x}, \frac{\partial}{\partial y}, \frac{\partial}{\partial x}\right)$ and $\nabla^2 \equiv \frac{\partial^2}{\partial x^2} + \frac{\partial^2}{\partial y^2} + \frac{\partial^2}{\partial z^2}$.

The basic state, which is assumed to be steady, is represented as follows:

$$\begin{aligned} &\mathbf{q} = \mathbf{q}_b = \mathbf{0}, \qquad T = T_b(z) = -\beta z + T_o, \\ &p = p_b(z), \qquad\quad \rho = \rho_b(z) = \rho_o(1+\alpha\beta z). \end{aligned} \tag{2.5}$$

Here, the subscript b denotes the basic state.

To investigate the stability or instability of the NSV fluid with couple stresses and rotational effects, we perturb the system with disturbances $\mathbf{q}'$, p', and θ in velocity, pressure, and temperature, respectively. The system of equations, with the apostrophes removed from the perturbed quantities, becomes:

$$\nabla\cdot\mathbf{q} = 0, \tag{2.6}$$

$$\rho_o\left(\frac{\partial \mathbf{q}}{\partial t} + (\mathbf{q}\cdot\nabla)\mathbf{q} - (\widehat{\lambda}\nabla^2)\frac{\partial \mathbf{q}}{\partial t}\right) = -\nabla p + (\mu - \mu'\nabla^2)\nabla^2\mathbf{q} + \rho_o g\alpha\theta\hat{\mathbf{k}} + 2\rho_o(\mathbf{q}\times\boldsymbol{\Omega}), \tag{2.7}$$

$$\frac{\partial\theta}{\partial t} + (\mathbf{q}\cdot\nabla)\theta = \beta w + \kappa\nabla^2\theta. \tag{2.8}$$

To non-dimensionalize the perturbed equations, we use following scales:

$$\begin{aligned} &z = dz^*, \quad t = \frac{\rho_o d^2}{\mu}t^*, \quad \mathbf{q} = \frac{\mu}{\rho_o d}\mathbf{q}^*, \quad p = \frac{\mu^2}{\rho_o d^2}p^*, \\ &\theta = \frac{\mu}{\rho_o d}\sqrt{\frac{\beta\mu}{\kappa g\alpha\rho_o}}\theta^*, \quad \widehat{\lambda} = t\nu\lambda^*, \end{aligned} \tag{2.9}$$

and the following non-dimensional parameters are introduced:

$$\mathrm{Ra} = \frac{\alpha g\beta d^4}{\nu\kappa}, \quad F = \frac{1}{\nu}\frac{\mu'}{\rho_o d^2}, \quad \mathrm{Pr} = \frac{\nu}{\kappa}, \quad \mathrm{Ta} = \left(\frac{2\Omega d^2}{\nu}\right)^2, \tag{2.10}$$

namely the Rayleigh number, the couple stress parameter, the Prandtl number, and the Taylor number respectively.

Using scales mentioned in (2.9) and non-dimensional parameters in (2.10) in the perturbed Eqs. (2.6)–(2.8), we derive the non-dimensional equations (dropping '*'s) as follows:

$$\nabla \cdot \mathbf{q} = 0, \tag{2.11}$$

$$\left(\frac{\partial \mathbf{q}}{\partial t} + (\mathbf{q}\cdot\nabla)\mathbf{q} - (\lambda\nabla^2)\frac{\partial \mathbf{q}}{\partial t}\right) = -\nabla p + \nabla^2\mathbf{q} - F\nabla^4\mathbf{q} + \mathrm{Ra}^{1/2}\theta\hat{\mathbf{k}} + \mathrm{Ta}^{1/2}(\mathbf{q}\times\hat{\mathbf{k}}), \tag{2.12}$$

$$\mathrm{Pr}\left(\frac{\partial \theta}{\partial t} + (\mathbf{q}\cdot\nabla)\theta\right) = \mathrm{Ra}^{1/2}\, w + \nabla^2\theta. \tag{2.13}$$

The curl of the velocity vector yields the vorticity, i.e., $\zeta = \hat{\mathbf{k}}\cdot\operatorname{curl}\mathbf{q}$, which represents the rotational motion within the fluid. By analyzing the third component of the vorticity equation, we gain insight into the behavior of rotational effects and the development of vertical structures, such as convective rolls or cells. By applying $\hat{\mathbf{k}}\cdot\operatorname{curl}$ on Eq. (2.12), and again applying $\hat{\mathbf{k}}\cdot\operatorname{curl}\operatorname{curl}$ on the same equation, we obtain:

$$(1-\lambda\nabla^2)\frac{\partial \zeta}{\partial t} + \hat{\mathbf{k}}\cdot\operatorname{curl}(\mathbf{q}\cdot\nabla)\mathbf{q} = \nabla^2\zeta - F\nabla^4\zeta + \mathrm{Ta}^{1/2}w_z, \tag{2.14}$$

$$(1-\lambda\nabla^2)\frac{\partial}{\partial t}(\nabla^2 w) + \hat{\mathbf{k}}\cdot\operatorname{curl}\operatorname{curl}(\mathbf{q}\cdot\nabla)\mathbf{q} = \nabla^4 w - F\nabla^6 w - \mathrm{Ta}^{1/2}\zeta_z + \mathrm{Ra}^{1/2}\nabla_1^2\theta. \tag{2.15}$$

Here, $\nabla_1^2 \equiv \frac{\partial^2}{\partial x^2} + \frac{\partial^2}{\partial y^2}$ represents the horizontal Laplacian. Additionally, $w_z = \frac{\partial w}{\partial z}$ and $\zeta_z = \frac{\partial \zeta}{\partial z}$.

The boundary conditions (BCs) are

$$w = 0,\ \theta = 0 \quad \text{at } z = 0, 1. \tag{2.16}$$

Other boundary conditions may vary depending on the specific nature of the surfaces at $z = 0$ and 1.

3. Nonlinear analysis

Nonlinear analysis investigates the intricate and interconnected factors in fluid flow that result in behaviors beyond the scope of linear equations. This approach assumes small yet finite perturbations during the analysis. On multiplying Eq. (2.14) by ζ, Eq. (2.15) by w and Eq. (2.13) by θ and then integrating over V (is the period cell), we get:

$$\frac{1}{2}\frac{d}{dt}(\|\zeta\|^2+\lambda\|\nabla\zeta\|^2) = -\langle\zeta\hat{\mathbf{k}}\cdot\operatorname{curl}(\mathbf{q}\cdot\nabla)\mathbf{q}\rangle - \|\nabla\zeta\|^2 - F\|\nabla^2\zeta\|^2 + \mathrm{Ta}^{1/2}\langle\zeta w_z\rangle, \tag{3.1}$$

$$\frac{1}{2}\frac{d}{dt}\big(\|\nabla w\|^2+\lambda\|\nabla^2 w\|^2\big) = -\|\nabla^2 w\|^2 - F\|\nabla^3 w\|^2 + \mathrm{Ta}^{1/2}\langle w\zeta_z\rangle + \mathrm{Ra}^{1/2}\langle\nabla_1 w\nabla_1\theta\rangle + \langle w\hat{\mathbf{k}}\cdot\operatorname{curl}\operatorname{curl}(\mathbf{q}\cdot\nabla)\mathbf{q}\rangle, \tag{3.2}$$

$$\frac{\mathrm{Pr}}{2}\frac{d}{dt}\|\theta\|^2 = -\|\nabla\theta\|^2 + \mathrm{Ra}^{1/2}\langle w\theta\rangle. \tag{3.3}$$

Here, $\nabla_1 \equiv \big(\frac{\partial}{\partial x}, \frac{\partial}{\partial y}\big)$, and $\langle\cdot\rangle$ and $\|\cdot\|$ denote the integration over V and L^2 norm on V, respectively.

By using (3.1), (3.2) and (3.3), we construct the energy $E(t)$, and the change in energy over time is

$$\frac{dE}{dt} = I_o + N_o - D_o. \tag{3.4}$$

Here,

$$E = \frac{\mathrm{Pr}}{2}\|\theta\|^2 + \frac{\lambda_1}{2}\|\nabla w\|^2 + \frac{\lambda\lambda_1}{2}\|\nabla^2 w\|^2 - \frac{\lambda_2}{2}\|\zeta\|^2 - \frac{\lambda\lambda_2}{2}\|\nabla\zeta\|^2, \tag{3.5}$$

$$I_o = \mathrm{Ra}^{1/2}\langle w\theta\rangle + \lambda_1\mathrm{Ra}^{1/2}\langle\nabla_1 w\nabla_1\theta\rangle + \lambda_1\mathrm{Ta}^{1/2}\langle w\zeta_z\rangle - \lambda_2\mathrm{Ta}^{1/2}\langle\zeta w_z\rangle, \tag{3.6}$$

$$D_o = \|\nabla\theta\|^2 + \lambda_1\|\nabla^2 w\|^2 + \lambda_1 F\|\nabla^3 w\|^2 - \lambda_2\|\nabla\zeta\|^2 - \lambda_2 F\|\nabla^2\zeta\|^2, \tag{3.7}$$

$$N_o = \lambda_2\langle\zeta\hat{\mathbf{k}}\cdot\operatorname{curl}(\mathbf{q}\cdot\nabla)\mathbf{q}\rangle + \lambda_1\langle w\hat{\mathbf{k}}\cdot\operatorname{curl}\operatorname{curl}(\mathbf{q}\cdot\nabla)\mathbf{q}\rangle, \tag{3.8}$$

where λ_1 and λ_2 are the positive coupling parameters. The terms I_o, D_o, and N_o represent the production, dissipation, and nonlinear interaction of energy, respectively, with I_o contributing to the energy input, D_o representing energy losses due to dissipation, and N_o accounting for additional energy transfers through nonlinear interactions.

Define

$$m = \max_{\mathrm{H}}\frac{I_o}{D_o},$$

where H is the space of admissible functions.

Then, $m < 1$ is required, for

$$\frac{dE}{dt} \le -D_o a_o + N_o. \tag{3.9}$$

Here, $a_o = 1 - m$ $(a_o > 0)$.

The generalized energy functional is now defined as

$$V_g(t) = E(t) + b_o E_1(t), \tag{3.10}$$

which is used to control the nonlinear terms and analyze nonlinear stability. In this case, b_o is a positive coupling parameter, and $E_1(t)$ represents the complementary energy, expressed as

$$E_1(t) = \frac{\lambda}{2}\|\nabla^2\mathbf{q}\|^2 + \frac{1}{2}\|\nabla\mathbf{q}\|^2 + \frac{\mathrm{Pr}}{2}\|\nabla\theta\|^2. \tag{3.11}$$

The evolution of $V_g(t)$ is given by

$$\frac{dV_g(t)}{dt} \le -a_o D_o + N_o + b_o I_1 - b_o D_1 + b_o N_1, \tag{3.12}$$

where

$$I_1 = 2\,\mathrm{Ra}^{1/2}\langle\nabla\theta\cdot\nabla w\rangle, \tag{3.13}$$

$$D_1 = \|\nabla^2\mathbf{q}\|^2 + F\|\nabla^3\mathbf{q}\|^2 + \|\nabla^2\theta\|^2, \tag{3.14}$$

$$N_1 = \langle\nabla^2\mathbf{q}\cdot(\mathbf{q}\cdot\nabla)\mathbf{q}\rangle + \mathrm{Pr}\langle(\mathbf{q}\cdot\nabla)\theta(\nabla^2\theta)\rangle. \tag{3.15}$$

We now revisit some embedding theorems and relevant results, expressed as follows:

$$\begin{aligned} &\sup|G| \le \mathrm{C}^*\|\nabla^2 G\|, \qquad \|\nabla w\| \le \|\nabla\mathbf{q}\|, \qquad G\in\{\mathbf{q},\theta\},\\ &\|K\|^2 \le \frac{1}{\pi^2}\|\nabla K\|^2, \qquad \langle\zeta\cdot\zeta'\rangle \le \frac{{\varepsilon_o}^2}{2}\|\zeta\|^2 + \frac{1}{2{\varepsilon_o}^2}\|\zeta'\|^2, \end{aligned} \tag{3.16}$$

where C^* is a constant that depends on the period cell V, and ϵ_o is constant. These theorems and results are discussed by STRAUGHAN in his monograph [31].

By substituting (3.7), (3.14), and inequalities (3.16) in (3.13) along with Young's and Cauchy–Schwarz inequalities, we derive:

$$b_o I_1 \le \frac{b_o{\varepsilon_o}^2}{2}D_1 + \frac{2b_o\,\mathrm{Ra}}{{\varepsilon_o}^2\pi^2}D_o. \tag{3.17}$$

Defining

$$D_2 = \frac{a_o}{2}D_o + \frac{b_o}{2}D_1, \tag{3.18}$$

and choosing

$$b_o = \frac{\pi^2 a_o}{4\,\mathrm{Ra}}, \qquad {\varepsilon_o}^2 = 1.$$

By applying Eq. (3.18), the inequality presented in (3.17) becomes

$$b_o I_1 \le D_2. \tag{3.19}$$

The nonlinear terms N_1 and N_o can be estimated using Eqs. (3.10), (3.11), (3.14), (3.18), and inequalities (3.16). These estimates are given as follows:

$$N_1 \leq \mathrm{C}^*\left(\frac{2}{b_o}\right)^{3/2}\frac{1}{\lambda^{1/2}}(\mathrm{Pr}^{1/2}+1){D_2}^{1/2}\cdot V_g, \tag{3.20}$$

$$N_o \leq \frac{\mathrm{C}^*}{\lambda^{1/2}}\left(\frac{2}{b_o}\right)^{3/2}\left(2\lambda_1+2\left(\frac{\lambda_2 b_o}{a_o}\right)^{1/2}\right){D_2}^{1/2}\cdot V_g. \tag{3.21}$$

Using inequalities (3.19), (3.20) and (3.21) in the inequality (3.12), we get

$$\frac{dV_g}{dt} \leq -D_2(1-\tilde{A}V_g), \tag{3.22}$$

where

$$\tilde{A} = \frac{\mathrm{C}^*}{\lambda^{1/2}}\left(\frac{2}{b_o}\right)^{3/2}\frac{1}{{D_2}^{1/2}}\left(b_o(\mathrm{Pr}^{1/2}+1)+2\lambda_1+2\left(\frac{\lambda_2 b_o}{a_o}\right)^{1/2}\right). \tag{3.23}$$

Here, it is important to note that $\tilde{A}$ depends on ${b_o}^{1/2}$ and $\lambda^{1/2}$. We derive sufficient conditions to ensure that the energy decays monotonically to zero. Now, to observe the behavior of energy decay, we need to perform some analysis and formulate the following theorem.

THEOREM.

Hypothesis: *Let* $V_g(0) < \tilde{A}^{-1}$ *and* $0 < m < 1$. *The value of* $\tilde{A}$ *is given by Eq.* (3.23).

Conclusion: *Then, there exists a constant* $\mathrm{K}^* > 0$ *such that, for all* $t \geq 0$, *the following inequality holds:*

$$V_g(t) \leq V_g(0)\exp(-\mathrm{K}^*(1-\tilde{A}V_g(0))t). \tag{3.24}$$

Proof. The inequality (3.22), and hypothesis ensures that

$$\frac{dV_g}{dt} \leq 0.$$

From the inequality (3.22), we obtain, using a recursion argument (see Appendix B), that:

$$\frac{dV_g}{dt} \leq -D_2(1-\tilde{A}V_g(0)), \quad \forall t \geq 0. \tag{3.25}$$

We need to demonstrate that there exists a number $\mathrm{K}^* > 0$ such that

$$\mathrm{K}^* V_g(t) \leq D_2. \tag{3.26}$$

In Eq. (3.10), using Eqs. (3.7), (3.14) and (3.18), we have the result

$$V_g(t) \leq \frac{1}{\pi^2}\left(1+\mathrm{Pr}+\pi^2\lambda\right)\left(1+\frac{1}{\pi^2}+\frac{\lambda}{F\pi^2}\right)\left(1+\frac{m}{1-m}\right)D_2.$$

Assume that

$$K_o \geq \frac{m}{1-m}, \quad \text{where } K_o > 0. \tag{3.27}$$

Let

$$K^* = \frac{\pi^2}{(1+\mathrm{Pr}+\pi^2\lambda)\big(1+\frac{1}{\pi^2}+\frac{\lambda}{F\pi^2}\big)(1+K_o)}.$$

Using this value of K^*, the inequality (3.25) becomes

$$\frac{dV_g}{dt} \leq -K^*(1-\tilde{A}V_g(0))V_g(t), \quad \forall t \geq 0. \tag{3.28}$$

On integrating the inequality (3.28), we get

$$V_g(t) \leq V_g(0)\exp(-K^*(1-\tilde{A}V_g(0))t).$$

This completes the proof. □

Variational principle

The variational principle is employed to derive governing equations by minimizing or maximizing a functional, often associated with energy or action. This method plays a vital role in nonlinear analysis, particularly for investigating the impact of small disturbances on a base flow. By applying the variational principle, eigenvalue problems can be formulated to evaluate the stability of flow structures, determine disturbance growth rates, and pinpoint stable or unstable regions in complex nonlinear systems.

We utilize the calculus of variations to assess the maximum problem at the critical argument $m = 1$. Taking transformations $w = \frac{\hat{w}}{\sqrt{\lambda_1}}$ and $\zeta = \frac{\hat{\zeta}}{\sqrt{\lambda_2}}$ for Eqs. (3.6) and (3.7), the associated Euler–Lagrange equation $\delta I_o - \delta D_o = 0$ gives the results:

$$\frac{\mathrm{Ra}^{1/2}}{\sqrt{\lambda_1}}\theta - {\lambda_1}^{1/2}\,\mathrm{Ra}^{1/2}\,{\nabla_1}^2\theta + \frac{(\lambda_1+\lambda_2)}{\sqrt{\lambda_1\lambda_2}}\mathrm{Ta}^{1/2}\zeta_z - 2\nabla^4 w + 2F\nabla^6 w = 0, \tag{3.29}$$

$$\frac{\mathrm{Ra}^{1/2}}{\sqrt{\lambda_1}}w - {\lambda_1}^{1/2}\,\mathrm{Ra}^{1/2}\,{\nabla_1}^2 w + 2\nabla^2\theta = 0, \tag{3.30}$$

$$\frac{(\lambda_1+\lambda_2)}{\sqrt{\lambda_1\lambda_2}}\mathrm{Ta}^{1/2}w_z + 2\nabla^2\zeta - 2F\nabla^4 Z = 0. \tag{3.31}$$

The plane tiling form is now assumed as

$$\{w, \theta, \zeta\} = \{W(z), \Theta(z), Z(z)\}\Psi(x, y), \tag{3.32}$$

where, Ψ denotes shape of the stability cell, (see CHANDRASEKHAR [1, p. 43–52]).

The plane tiling form is a mathematical representation used in the stability analysis and fluid dynamics to describe spatially periodic perturbations. It expresses perturbations in terms of separable functions, where the depth-dependent components $W(z)$, $\Theta(z)$ and $Z(z)$ capture variations in the vertical direction, while the function $\Psi(x, y)$ defines the horizontal spatial structure. The function $\Psi(x, y)$ satisfies $\nabla_1^2\Psi = -a^2\Psi$, where a is the wave number, determining the periodicity of the tiling pattern. This equation ensures that $\Psi(x, y)$ exhibits sinusoidal or exponential behavior, characterizing the repeating structure of instability modes.

Using the plane tiling form (3.32) in Eqs. (3.29)–(3.31), the eigenvalue problem we obtain takes the form:

$$\begin{aligned} 2(D^2 - a^2)^2 W - 2F(D^2 - a^2)^3 W - \left(\frac{\mathrm{Ra}}{\lambda_1}\right)^{1/2}\Theta \\ - {\lambda_1}^{1/2}\,\mathrm{Ra}^{1/2}\,a^2\Theta - \frac{(\lambda_1 + \lambda_2)}{\sqrt{\lambda_1\lambda_2}}\mathrm{Ta}^{1/2} DZ = 0, \end{aligned} \tag{3.33}$$

$$2(D^2 - a^2)\Theta + \left(\frac{\mathrm{Ra}}{\lambda_1}\right)^{1/2} W + {\lambda_1}^{1/2}\,\mathrm{Ra}^{1/2}\,a^2 W = 0, \tag{3.34}$$

$$2(D^2 - a^2)Z - 2F(D^2 - a^2)^2 Z + \frac{(\lambda_1 + \lambda_2)}{\sqrt{\lambda_1\lambda_2}}\mathrm{Ta}^{1/2} DW = 0, \tag{3.35}$$

with the boundary conditions:

for free-free surfaces

$$W = D^2W = D^4W = \Theta = DZ = D^3Z = 0 \quad \text{at } z = 0, 1; \tag{3.36}$$

for rigid-free surfaces

$$\begin{aligned} &W = DW = D^3W = \Theta = Z = D^2Z = 0 \qquad \text{at } z = 0, \\ &W = D^2W = D^4W = \Theta = DZ = D^3Z = 0 \qquad \text{at } z = 1; \end{aligned} \tag{3.37}$$

for rigid-rigid surfaces

$$W = DW = D^3W = \Theta = Z = D^2Z = 0 \quad \text{at } z = 0, 1. \tag{3.38}$$

Here, $D \equiv \frac{d}{dz}$ is the derivative with respect to the vertical coordinate z.

4. Linear analysis

In linear analysis, the system is subjected to infinitesimally small disturbances, allowing the focus to remain on the first-order terms in the perturbation equations. This method assumes that the deviations are minimal, enabling the prediction of instability. It provides valuable insights into flow behavior under small perturbations without requiring a full nonlinear analysis.

We linearize the non-dimensional perturbed Eqs. (2.13)–(2.15) and for the analysis of linear instability by omitting nonlinear terms. Utilizing the normal mode analysis method, we assume solutions of the form $w(\mathbf{x},t) = w(\mathbf{x})e^{\sigma t}$, $\theta(\mathbf{x},t) = \theta(\mathbf{x})e^{\sigma t}$. Subsequently, the linearized non-dimensional equations are derived as follows:

$$\Pr \sigma\theta = \nabla^2\theta + \mathrm{Ra}^{1/2}\, w, \tag{4.1}$$

$$\sigma(1-\lambda\nabla^2)\zeta = \nabla^2\zeta - F\nabla^4\zeta + \mathrm{Ta}^{1/2} w_z, \tag{4.2}$$

$$\sigma(1-\lambda\nabla^2)\nabla^2 w = \nabla^4 w - F\nabla^6 w + \mathrm{Ra}^{1/2}\nabla_1^2\theta - \mathrm{Ta}^{1/2}\zeta_z. \tag{4.3}$$

Here, σ represents the growth rate.

Using the plane tiling form (3.32) in Eqs. (4.1)–(4.3), we have the following eigenvalue problem

$$\Pr \sigma\Theta = (D^2-a^2)\Theta + \mathrm{Ra}^{1/2}\, W, \tag{4.4}$$

$$\sigma Z - \sigma\lambda(D^2-a^2)Z = (D^2-a^2)Z - F(D^2-a^2)^2 Z + \mathrm{Ta}^{1/2} DW, \tag{4.5}$$

$$\begin{aligned}\sigma(D^2-a^2)W - \sigma\lambda(D^2-a^2)^2 W = (D^2-a^2)^2 W - F(D^2-a^2)^3 W \\ - a^2\,\mathrm{Ra}^{1/2}\,\Theta - \mathrm{Ta}^{1/2} DZ,\end{aligned} \tag{4.6}$$

with the same boundary conditions as those provided in (3.36)–(3.38).

5. Method of solution

The single-term Galerkin method, a well-established approach in numerical analysis, has been utilized to solve eigenvalue problems. CHANDRASEKHAR [1] derived the exact solution for free-free boundary conditions. For the cases involving rigid-rigid and rigid-free boundary conditions, approximate solutions that satisfy the corresponding boundary conditions are considered. In this context, the set of solutions

$$W = \sum_{i=1}^{n} G_i W_i, \tag{5.1}$$

$$\Theta = \sum_{i=1}^{n} H_i \Theta_i, \tag{5.2}$$

$$Z = \sum_{i=1}^{n} I_i Z_i, \tag{5.3}$$

where W_i, Θ_i, Z_i are the basis functions and G_i, H_i, I_i are the constants, and i denotes the iteration number.

For free-free bounding surfaces

As per boundary conditions (3.36), the set of exact solutions are as follows [1]:

$$W_i = \sin(i\pi z), \quad \Theta_i = \sin(i\pi z), \quad Z_i = \left(\frac{2\Omega d}{\nu}\right)\left(\frac{i\pi}{i^2\pi^2 + a^2}\right)\cos(i\pi z). \tag{5.4}$$

For rigid-free bounding surfaces

As per boundary conditions (3.37), the basis functions are as follows [13, 32]:

$$\begin{aligned} W_i &= -z^{2i} + 3.25z^{2i+2} - 3.05z^{2i+3} + 0.8z^{2i+4}, \\ \Theta_i &= z^i - 2z^{i+2} + z^{i+3}, \quad Z_i = 8z^i - 4z^{i+2} + z^{i+3}. \end{aligned} \tag{5.5}$$

For rigid-rigid bounding surfaces

As per boundary conditions (3.38), the basis functions are as follows [13, 32]:

$$\begin{aligned} W_i &= -0.5z^{2i} + 2.5z^{2i+2} - 3z^{2i+3} + z^{2i+4}, \\ \Theta_i &= z^i - 2z^{i+2} + z^{i+3}, \quad Z_i = z^i - \frac{2}{3}z^{i+2} - \frac{4}{3}z^{i+3} + z^{i+4}. \end{aligned} \tag{5.6}$$

Using the solutions described in forms (5.1)–(5.3) into the eigenvalue problems of both analyses, and employing the Galerkin technique, yields a system of linear homogeneous equations:

$$\mathrm{D}_{ji}G_i + \mathrm{E}_{ji}H_i + \mathrm{F}_{ji}I_i = 0, \tag{5.7}$$

$$\mathrm{P}_{ji}G_i + \mathrm{Q}_{ji}H_i + \mathrm{R}_{ji}I_i = 0, \tag{5.8}$$

$$\mathrm{S}_{ji}G_i + \mathrm{T}_{ji}H_i + \mathrm{U}_{ji}I_i = 0. \tag{5.9}$$

The set of the above equations possesses a nontrivial solution when the determinant of the coefficient matrix is zero, which can be expressed as

$$\begin{vmatrix} \mathrm{D}_{ji} & \mathrm{E}_{ji} & \mathrm{F}_{ji} \\ \mathrm{P}_{ji} & \mathrm{Q}_{ji} & \mathrm{R}_{ji} \\ \mathrm{S}_{ji} & \mathrm{T}_{ji} & \mathrm{U}_{ji} \end{vmatrix} = 0. \tag{5.10}$$

Using (5.10), we get the value of Rayleigh numbers $\mathrm{Ra_N}$ (for nonlinear) and $\mathrm{Ra_L}$ (for linear).

5.1. The case of nonlinear analysis

The Rayleigh numbers ($\mathrm{Ra_N}$) for three different bounding surfaces were calculated using the single-term Galerkin method with the help of Mathematica software. The resulting $\mathrm{Ra_N}$ values are expressed in terms of the parameters a, Ta, and F. To determine the optimal values of λ_1 and λ_2, the conditions $\frac{d\,\mathrm{Ra_N}}{d\lambda_1} = 0$ and $\frac{d\,\mathrm{Ra_N}}{d\lambda_2} = 0$ were applied, respectively. It was found that the optimal values for all bounding surfaces considered in this study are $\lambda_1 = \lambda_2 = \frac{1}{a^2}$. Substituting these optimal values of λ_1 and λ_2 into the expression of $\mathrm{Ra_N}$, we obtained the final result.

5.2. The case of linear analysis

The linear analysis predicts the threshold for the onset of stationary or oscillatory convection modes. To identify the stationary and oscillatory convection modes, we substitute $\sigma = \iota\omega$ in the Rayleigh numbers ($\mathrm{Ra_L}$) obtained from eigenvalue problem (4.4)–(4.6), using the single-term Galerkin method. This substitution yields the Rayleigh number ($\mathrm{Ra_L}$) in the form

$$\mathrm{Ra_L} = \mathrm{Ra_r} + \iota\omega\,\mathrm{Ra_i}, \tag{5.11}$$

where ω represents the frequency distribution, and $\mathrm{Ra_i}$ and $\mathrm{Ra_r}$ are the imaginary and real parts of $\mathrm{Ra_L}$, respectively.

Since the Ra is a physical quantity, it must be real. Consequently, Eq. (5.11) yields two possible scenarios: either $\omega = 0$, corresponding to stationary convection, or $\omega \neq 0$ with $\mathrm{Ra_i} = 0$, which indicates the occurrence of oscillatory convection.

5.2.1. Stationary convection When $\omega = 0$, it indicates the absence of oscillatory convection, and the system exhibits stationary convection modes. In this case, the stationary Rayleigh number ($\mathrm{Ra_{st}}$) is given by the expression in Eq. (5.11), which is identical to $\mathrm{Ra_N}$. The value of $\mathrm{Ra_{st}}$ is expressed in terms of a, Ta, and F.

5.2.2. Oscillatory convection The occurrence of oscillatory convection requires ω^2 to be positive [31]. The condition $\mathrm{Ra_i} = 0$ yields an expression for the oscillation frequency ω^2. Using Mathematica software, we explored the range of wave numbers that support the onset of oscillatory modes for the varying Taylor numbers (Ta), the couple stress parameter (F), and the Kelvin–Voigt coefficients (λ), while keeping certain non-dimensional parameters fixed. Within this range, the

corresponding values of ω^2 were determined. These values were then utilized to compute the Rayleigh number for oscillatory modes ($\mathrm{Ra}_{\mathrm{osc}}$) by substituting ω^2 into the real part of Ra_{L}.

6. Results and discussion

The Rayleigh numbers, Ra_{N} and $\mathrm{Ra}_{\mathrm{st}}$ were calculated for various boundary conditions using the single-term Galerkin method with the help of Mathematica software.

For free-free boundary conditions, the Rayleigh number we obtain is

$$\mathrm{Ra}_{\mathrm{N}} = \frac{\begin{pmatrix} a^{10}F^2 + a^8F(2+5F\pi^2) + a^2\pi^4(3+8F\pi^2+5\pi^4F^2) \\ +a^6(1+8F\pi^2+10F^2\pi^4) + a^4\pi^2(3+12F\pi^2 \\ +10F^2\pi^4) + \pi^2(\pi^4+2F\pi^6+F^2\pi^8+\mathrm{Ta}) \end{pmatrix}}{a^2(1+a^2F+\pi^2F)} \tag{6.1}$$
$$= \mathrm{Ra}_{\mathrm{st}}\,.$$

For rigid-rigid boundary conditions, the Rayleigh number we obtain is

$$\mathrm{Ra}_{\mathrm{N}} = \frac{\begin{pmatrix} 52249.2+2.63415\times10^6F+2.17672\times10^6F^2+1.0381a^{12}F^2 \\ +a^{10}F(2.07619+71.1017F)+a^8(1.0381+118.457F \\ +3098.22F^2)+a^6(47.3552+4127.3F+81753.6F^2) \\ +a^4(1162.75+81610.6F+1.15248\times10^6F^2)+0.589366\,\mathrm{Ta} \\ +a^2(13155+764506F+8.01766\times10^6F^2+0.059707\,\mathrm{Ta}) \end{pmatrix}}{a^2(10.0038+104.191F+a^4F+a^2(1+20.0076F))} \tag{6.2}$$
$$= \mathrm{Ra}_{\mathrm{st}}\,.$$

For rigid-free boundary conditions, the Rayleigh number we obtain is

$$\mathrm{Ra}_{\mathrm{N}} = \frac{\begin{pmatrix} 6333.39+156791F+348709F^2+1.07057a^{12}F^2 \\ +a^{10}F(2.14114+54.4577F)+a^8(1.07057+93.4048F \\ +1410.31F^2)+a^6(38.947+1982.2F+19524.1F^2) \\ +a^4(603.649+21683.9F+130873F^2)+13.1558\,\mathrm{Ta} \\ +a^2(3835.03+106296F+364557F^2+1.33278\,\mathrm{Ta}) \end{pmatrix}}{a^2(2.46774+6.09677F+a^4F+a^2(1+4.93548F))} \tag{6.3}$$
$$= \mathrm{Ra}_{\mathrm{st}}\,.$$

Here, the identical Rayleigh numbers indicate the non-existence of subcritical instabilities. This finding strongly supports the global stability.

Figure 2 illustrates the variations of $\mathrm{Ra_N}$ and $\mathrm{Ra_{st}}$ and a across various combinations of boundary conditions, namely free-free, rigid-rigid, and rigid-free, at $\mathrm{Ta} = 1000$ and $F = 0.1$. This figure illustrates that the $\mathrm{Ra_{st}}$ aligns with the $\mathrm{Ra_N}$. The overlapping curves confirm the global stability across different boundary conditions. It has also been noted that the NSV fluid demonstrates higher stability when enclosed by rigid boundaries, whereas it exhibits the lowest stability with free boundaries.

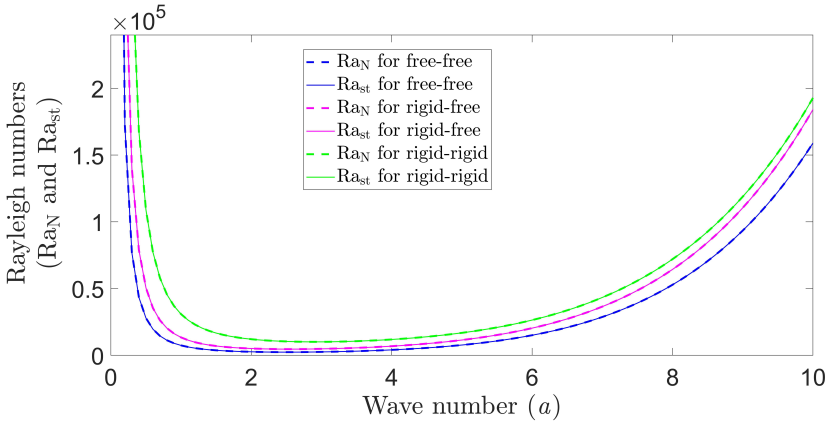

FIG. 2. Rayleigh number ($\mathrm{Ra_N}$ and $\mathrm{Ra_{st}}$) vs wave number (a) for various combinations of bounding surfaces at $F = 0.1$ and $\mathrm{Ta} = 1000$.

Figure 3 illustrates the variation of $\mathrm{Ra_{st}}$ and $\mathrm{Ra_{osc}}$ with a for free-free boundary conditions. In Fig. 3(a), as the couple stress parameter (F) increases, the range of wave numbers supporting oscillatory convection narrows: from $0 < a < 2.02$ for $F = 0.05$ to $0 < a < 0.34$ for $F = 0.15$. This delays the onset of oscillatory convection, indicating a stabilizing effect. For stationary convection, the onset is similarly delayed as F increases, reflecting the stabilizing role of the couple stress parameter. Figure 3(b) shows that as the Taylor number (Ta) increases, the wave number range for oscillatory convection broadens: from $0 < a < 1.26$ for $\mathrm{Ta} = 1000$ to $0 < a < 4.91$ for $\mathrm{Ta} = 100\,000$. This expansion is accompanied by a delay in convection onset, highlighting the stabilizing effect of rotation. Figure 3(c) reveals that higher Kelvin–Voigt parameters (λ) also expand the oscillatory convection range: from $0 < a < 1.26$ for $\lambda = 1$ to $0 < a < 1.50$ for $\lambda = 3$, while the stationary Rayleigh number remains unaffected. An increase in λ also advances the onset of convection, indicating the destabilizing effect of viscoelasticity. Overall, the couple stress parameter contracts the oscillatory convection range, while the Taylor number and Kelvin–Voigt parameter expand it.

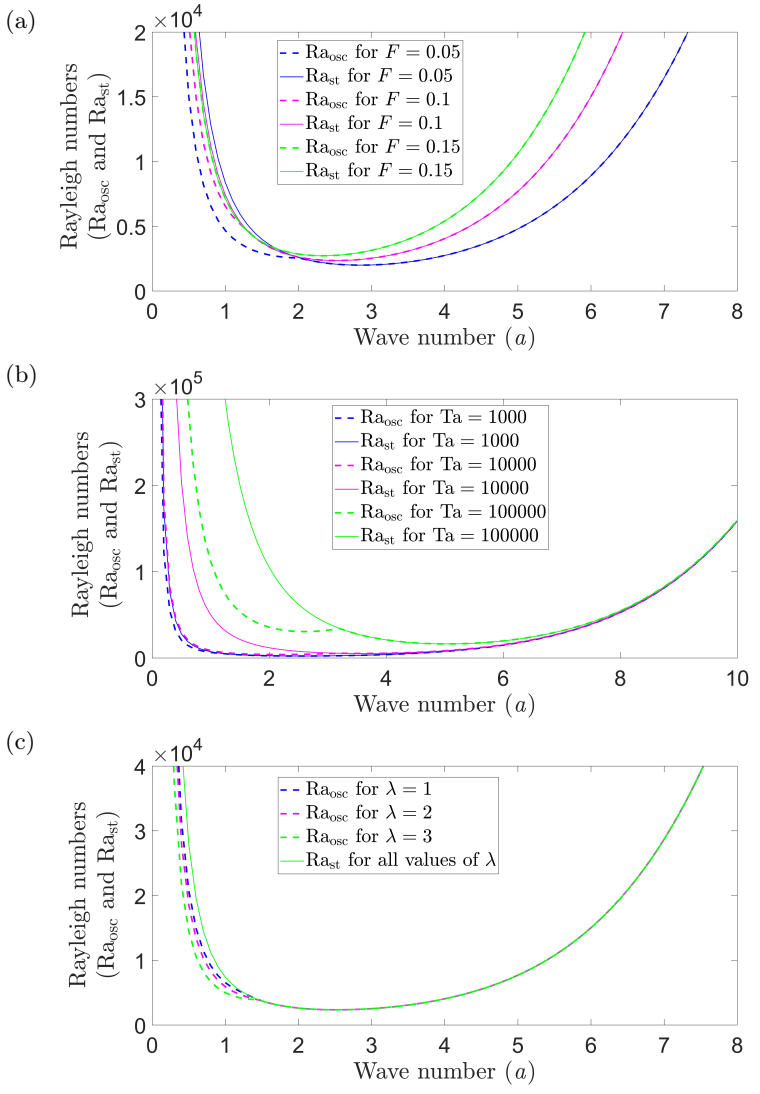

FIG. 3. Variations of Rayleigh numbers ($\mathrm{Ra_{st}}$ and $\mathrm{Ra_{osc}}$) with wave number (a) at various values of, (a) F at Ta = 1000, Pr = 1, $\lambda = 1$, (b) Ta at $F = 0.1$, Pr = 1, $\lambda = 1$, (c) λ at $F = 0.1$, Ta = 1000, Pr = 1 (for free-free boundary conditions).

Figure 4 illustrates the variation of the Rayleigh numbers ($\mathrm{Ra_{st}}$ and $\mathrm{Ra_{osc}}$) with the wave number (a) under rigid-rigid boundary conditions for different values of the couple stress parameter (F), the Taylor number (Ta), and the Kelvin–Voigt parameter λ. Each subfigure represents the variation of the Rayleigh numbers with respect to the wave number for different values of one parameter, while keeping the others fixed. In all cases, oscillatory convection is absent as $\mathrm{Ra_{st}}$ and

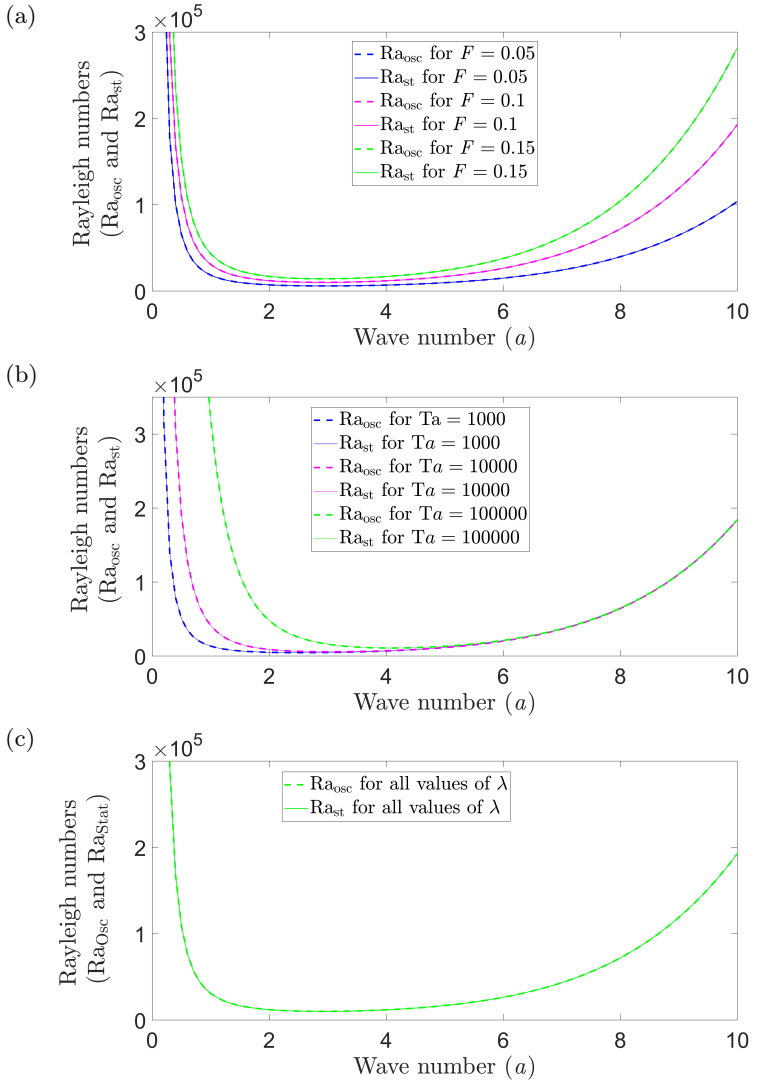

FIG. 4. Variations of Rayleigh numbers ($\mathrm{Ra_{st}}$ and $\mathrm{Ra_{osc}}$) with wave number (a) at various values of, (a) F at Ta = 1000, Pr = 1, $\lambda = 1$, (b) Ta at $F = 0.1$, Pr = 1, $\lambda = 1$, (c) λ at $F = 0.1$, Ta = 1000, Pr = 1 (for rigid-rigid boundary conditions).

$\mathrm{Ra_{osc}}$ coincide, confirming purely stationary convection. The Rayleigh number initially decreases with an increasing wave number, reaching a minimum at the most unstable mode before rising again, indicating that higher wave numbers require stronger thermal driving forces for convection. In Fig. 4(a), increasing F raises the Rayleigh numbers for all wave numbers, demonstrating the stabilizing effect of couple stresses, which introduce viscosity-like microstructural interac-

tions that suppress convection. Similarly, Fig. 4(b) shows that increasing Ta stabilizes the system by increasing the Rayleigh numbers, highlighting the stabilizing effect of rotation on convective motion. Figure 4(c) reveals that λ has no significant influence on convection onset, as $\mathrm{Ra_{st}}$ and $\mathrm{Ra_{osc}}$ remain identical for all values, reinforcing the dominance of stationary convection.

Figure 5 shows the variation of $\mathrm{Ra_{st}}$ and $\mathrm{Ra_{osc}}$ with a for rigid-free boundary conditions. In Fig. 5(a), the oscillatory convection modes for the rotating

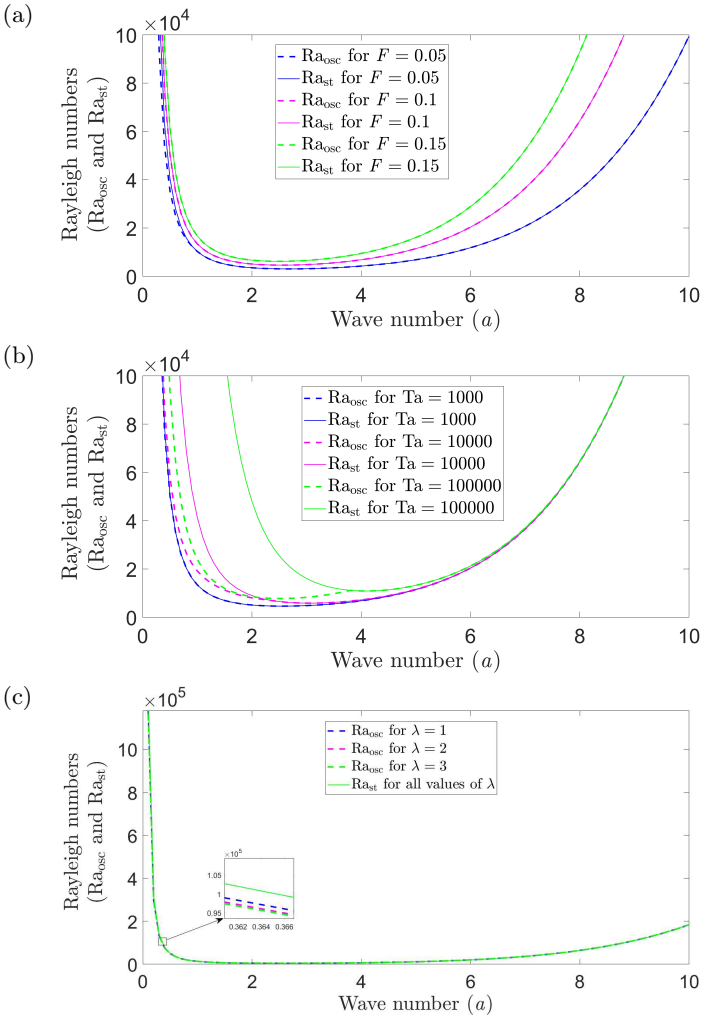

FIG. 5. Variations of Rayleigh numbers ($\mathrm{Ra_{st}}$ and $\mathrm{Ra_{osc}}$) with wave number (a) at various values of, (a) F at Ta = 1000, Pr = 1, $\lambda = 1$, (b) Ta at $F = 0.1$, $\lambda = 1$, Pr = 1, (c) λ at $F = 0.1$, Ta = 1000, Pr = 1 (for rigid-free boundary conditions).

NSV fluid are observed within the wave number ranges of $0 < a < 0.92$ for $F = 0.05$, $0 < a < 0.54$ for $F = 0.1$, and no oscillatory convection at $F = 0.15$. As the couple stress parameter (F) increases, the range for oscillatory convection decreases and its onset is delayed, indicating a stabilizing effect. Figure 5(b) shows that as the Taylor number (Ta) increases from 1000 to 100 000, the range for oscillatory convection expands (from $0 < a < 0.54$ for Ta = 1000 to $0 < a < 3.79$ for Ta = 100 000), and convection onset is delayed, indicating that rotation also stabilizes the fluid. Figure 5(c) illustrates that increasing λ broadens the spectrum of a for oscillatory convection, from $0 < a < 0.54$ for $\lambda = 1$ to $0 < a < 0.62$ for $\lambda = 3$, while $\mathrm{Ra_{st}}$ remains unaffected. A higher λ also advances convection onset, highlighting the destabilizing effect of viscoelasticity.

To identify the critical Rayleigh numbers, which indicates the point at which convection begins, we first determined the critical wave numbers by solving the condition $\frac{d\,\mathrm{Ra_N}}{da} = 0$ for Eqs. (6.1)–(6.3). We then substituted these critical wave numbers into Eqs. (6.1)–(6.3), to calculate the corresponding critical Rayleigh numbers. Based on the numerical critical Rayleigh numbers, we present the results graphically.

Figure 6 shows the variations of the critical Rayleigh number ($\mathrm{Ra_c}$) and the couple stress parameter (F) across different combinations of bounding surfaces (i.e., free-free, rigid-rigid, rigid-free) at Ta = 1000. The curves in the figure represent the onset of convection. The region below each curve indicates conditions under which the rotating NSV fluid remains stable, while the region above each curve signifies instability. The figure also highlights that an increase in the couple stress parameter (F) leads to a corresponding increase in the critical Rayleigh number ($\mathrm{Ra_c}$), implying that the couple stresses delays the onset of convection,

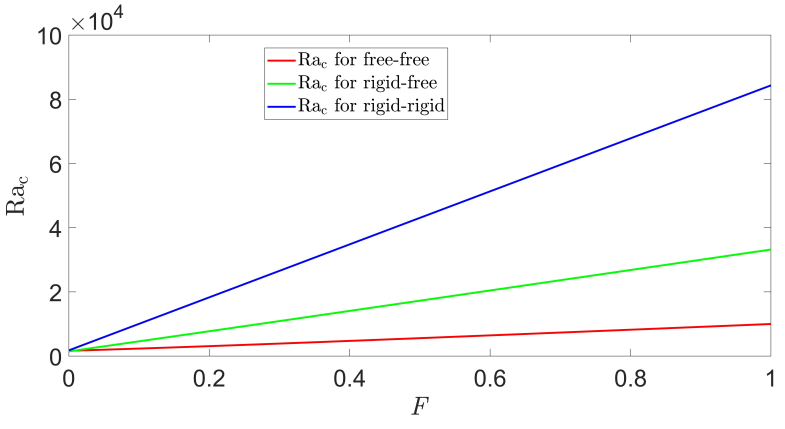

FIG. 6. Critical Rayleigh number ($\mathrm{Ra_c}$) vs couple stress parameter (F) for different combinations of bounding surfaces at Ta = 1000.

exerting a stabilizing effect. Moreover, the figure clearly shows that the critical value of the Rayleigh number is higher for rigid-rigid bounding surfaces compared to free-free and rigid-free bounding surfaces. This indicates that the NSV fluid is more thermally stable when confined by rigid boundaries and least stable when both surfaces are free.

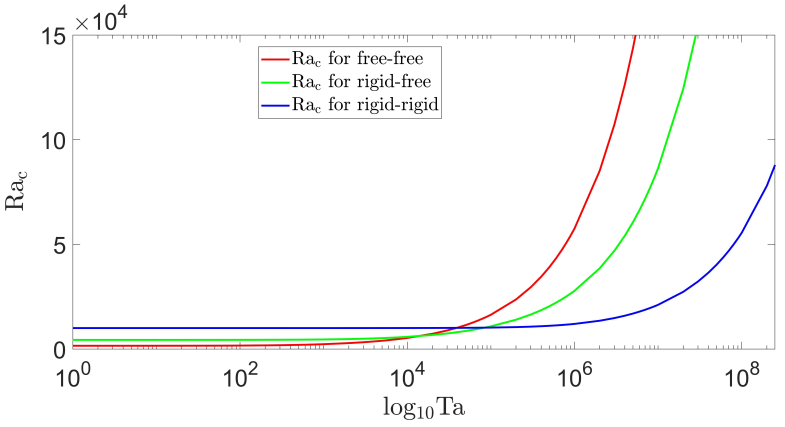

FIG. 7. Variation of critical Rayleigh number ($\mathrm{Ra_c}$) and Taylor number (Ta) for different combinations of bounding surfaces at $F = 0.1$.

Figure 7 depicts the variations of the critical Rayleigh number ($\mathrm{Ra_c}$) and the Taylor number (Ta) across different combinations of bounding surfaces (i.e., free-free, rigid-rigid, rigid-free) at $F = 0.1$. The figure clearly shows that for the Taylor numbers ranging from 0 to 4×10^4, the critical Rayleigh number is highest for rigid-rigid boundaries, followed by free-free, and then rigid-free boundaries. This suggests that in this range, the NSV fluid exhibits the greatest thermal stability when confined by rigid-rigid boundaries. Beyond a Taylor number of 4×10^4, the free-free configuration exhibits a higher critical Rayleigh number compared to both the rigid-free and rigid-rigid configurations. Between 4×10^4 and 8.5×10^4, the rigid-rigid boundaries still display a higher critical Rayleigh number than the rigid-free configuration, but beyond 8.5×10^4, the rigid-free configuration surpasses the rigid-rigid one, though it remains lower than the free-free configuration. In conclusion, within the Taylor number range of 0 to 4×10^4, the NSV fluid demonstrates superior thermal stability with rigid-rigid boundaries compared to the other boundary conditions. For the Taylor numbers exceeding 4×10^4, the NSV fluid becomes most thermally stable with free-free boundaries. Additionally, for the Taylor numbers ranging from 0 to 1.48×10^4, the NSV fluid is least stable under free-free boundary conditions. In the intermediate range, from 1.48×10^4 to 8.5×10^4, the system becomes least stable with rigid-free boundaries. However, beyond 8.5×10^4, the rigid-rigid con-

figuration emerges as the least stable, while the free-free boundary configuration consistently demonstrates the highest stability across all Taylor numbers.

7. Conclusions

The above analysis leads to the following conclusions:

- The Kelvin–Voigt and couple stress parameters significantly affect energy decay in the system. However, only the Taylor number and the couple stress parameter govern the stationary Rayleigh number. All three parameters – Kelvin–Voigt, couple stress, and Taylor number – play an important role in influencing oscillatory convection behavior and stability transitions.
- The Rayleigh numbers for the nonlinear analysis and stationary convection are identical, which indicates the non-existence of subcritical instabilities.
- The oscillatory convection mode arises due to the effects of couple stresses, rotation, and viscoelasticity.
- Fluid confined between rigid-rigid bounding surfaces exhibits enhanced thermal stability. This configuration is particularly effective for convection in the rotating NSV fluid, as it promotes a more stable thermal environment and influences the convection process positively.
- Couple stresses and rotational effects effectively delay the onset of thermal convection, illustrating their stabilizing impact on the fluid system by dampening convective disturbances. In contrast, viscoelasticity accelerates convection onset, revealing its destabilizing influence specifically on oscillatory convection, while not affecting stationary convection.

The findings of this study provide valuable insights into the stability and thermal management of NSV fluids under the influence of rotation and couple stresses. These insights are particularly significant for industrial applications such as cooling systems and aerospace engineering. In industrial cooling systems, including power plants and advanced electronic devices, the stabilizing effects of couple stresses and rotational forces enhance heat exchanger designs, ensuring efficient thermal dissipation and system durability. Similarly, in aerospace applications, where precise thermal regulation is vital in systems like jet engines and rotating turbines, the study's findings can guide the development of advanced cooling mechanisms to maintain reliable performance under extreme thermal loads.

In renewable energy and environmental engineering, the stability analysis of NSV fluids under rotational effects and couple stresses is instrumental in optimizing thermal energy systems. For example, in solar thermal power plants

and geothermal systems, the stabilizing impact of these parameters improves the efficiency of heat transfer and storage processes. Furthermore, environmental applications such as pollutant removal systems benefit from enhanced control over fluid stability in configurations subjected to rotational or cyclic forces. The study's emphasis on fluid behavior in rigid boundary setups also supports the development of robust designs for such processes, ensuring operational reliability and effectiveness.

The research findings have further implications for biomedical devices, civil engineering, and material development. In biomedical engineering, the stabilizing properties of couple stresses can enhance the efficiency and reliability of precision fluid systems such as dialysis machines and drug delivery devices. In civil engineering, insights into the thermal stability of NSV fluids can support the design of geothermal foundations and energy-efficient materials for infrastructure. Additionally, the study contributes to the development of thermally and mechanically stable viscoelastic materials for advanced applications, ensuring optimal performance in systems requiring precise thermal and fluid control. These findings collectively advance knowledge and innovation in engineering, energy systems, and environmental technology.

Appendix A

Derivation of the equation of motion for the NSV fluid in the presence of couple stresses

The constitutive equations proposed by Stokes [14] are

$$T_{(ij)} = (-p + \Lambda D_{kk})\delta_{ij} + 2\mu D_{ij}, \tag{A.1}$$

$$T_{[ij]} = -2\eta W_{ij,kk} - \frac{\rho}{2}\epsilon_{ijs}G_s, \tag{A.2}$$

$$M_{ij} = 4\eta\omega_{j,i} + 4\eta'\omega_{i,j}, \tag{A.3}$$

where

$$D_{ij} = \frac{1}{2}(q_{i,j} + q_{j,i}), \quad W_{ij} = \frac{1}{2}(q_{i,j} - q_{j,i}), \quad \omega_i = \frac{1}{2}\epsilon_{ijk}q_{k,j}. \tag{A.4}$$

Here, T_{ij}, $T_{(ij)}$, $T_{[ij]}$, M_{ij}, D_{ij}, W_{ij}, ω_i, G_s, ϵ_{ijk}, $\mathbf{q}$, and ρ are stress tensors, symmetric part of T_{ij}, anti-symmetric part of T_{ij}, couple stress tensor, deformation tensor, the vorticity tensor, the vorticity vector, body couple, the alternating unit tensor, velocity field, the density, and material constant, respectively. The dimensions of material constant Λ and μ are those of viscosity whereas dimensions of η and η' are those of momentum.

The stress for couple stresses in fluids

$$\begin{aligned} T_{ij} &= T_{(ij)} + T_{[ij]} \\ &= \big((-p + \Lambda D_{kk})\delta_{ij} + 2\mu D_{ij}\big) + \left(-2\eta W_{ij,kk} - \frac{\rho}{2}\epsilon_{ijs}G_s\right) \\ &= -p\delta_{ij} + \Lambda D_{kk}\delta_{ij} + 2\mu D_{ij} - 2\eta W_{ij,kk} - \frac{\rho}{2}\epsilon_{ijs}G_s \\ &= -p\delta_{ij} + \Lambda q_{k,k}\delta_{ij} + \mu(q_{i,j} + q_{j,i}) - \eta(q_{i,j} - q_{j,i}) - \frac{\rho}{2}\epsilon_{ijs}G_s. \end{aligned}$$

Now, in terms of the stress T_{ij}, we can write down the hydrodynamical equation of motion for the Navier–Stokes–Voigt fluid [1, 7] as

$$\begin{aligned} \text{(A.5)}\quad \rho_o(1 - \widehat{\lambda}\nabla^2)\frac{\partial q_i}{\partial t} + \rho_o q_j \frac{\partial q_i}{\partial x_j} &= \rho_o g\alpha T k_i + \frac{\partial}{\partial x_j}T_{ij} \\ &= \rho_o g\alpha T k_i - \frac{\partial p}{\partial x_i} + \frac{\partial}{\partial x_j}\bigg(\Lambda q_{k,k}\delta_{ij} \\ &\quad + \mu(q_{i,j} + q_{j,i}) - \eta(q_{i,j} - q_{j,i}) - \frac{\rho}{2}\epsilon_{ijs}G_s\bigg). \end{aligned}$$

For an incompressible NSV fluid in the absence of a body couple, Eq. (A.5) becomes:

$$\text{(A.6)}\qquad \rho_o\big(1 - \widehat{\lambda}\nabla^2\big)\frac{\partial q_i}{\partial t} + \rho_o q_j \frac{\partial q_i}{\partial x_j} = \rho_o g\alpha T k_i - \frac{\partial p}{\partial x_i} + \mu q_{i,jj} - \eta(q_{i,jj})_{kk}.$$

The assumption of the absence of a body couple implies that no external torques or moments are acting on the fluid. This simplification allows the governing equations to focus on other forces, such as pressure gradients and viscous effects, without the added complexity of torque-induced stresses.

In the vector form, A.6 can be written as

$$\text{(A.7)}\qquad \rho_o\left((1 - \widetilde{\lambda}\nabla^2)\frac{\partial}{\partial t} + \mathbf{q}\cdot\nabla\right)\mathbf{q} = -\nabla p + \rho_o g\alpha T\hat{\mathbf{k}} + \mu\nabla^2\mathbf{q} - \mu'\nabla^4\mathbf{q}.$$

Here, μ' is responsible for couple stress properties. This is the equation of motion for the NSV fluid in the presence of couple stresses. The equation of motion for rotating NSV fluid in the presence of couple stresses becomes:

$$\rho_o\left((1 - \widehat{\lambda}\nabla^2)\frac{\partial}{\partial t} + \mathbf{q}\cdot\nabla\right)\mathbf{q} = -\nabla p + (\mu - \mu'\nabla^2)\nabla^2\mathbf{q} + \rho_o g\alpha T\hat{\mathbf{k}} + 2\rho_o(\mathbf{q}\times\boldsymbol{\Omega}).$$

Appendix B

Derivation of Eq. (3.25) from inequality (3.22) using a recursive argument

We have

$$\frac{dV_g}{dt} \leq -D_2(1-\tilde{A}V_g). \tag{B.1}$$

Let us consider small time steps Δt and define discrete time points:

$$t_n = n\Delta t, \quad n = 0, 1, 2\ldots, \tag{B.2}$$

where $t_o = 0$ corresponds to the initial condition $V_g(0)$. For a small interval Δt, we approximate the derivative as

$$\frac{V_g(t_{n+1}) - V_g(t_n)}{\Delta t} \approx \left.\frac{dV_g}{dt}\right|_{t=t_n}.$$

Using (B.1), we get:

$$\begin{aligned} &\frac{V_g(t_{n+1}) - V_g(t_n)}{\Delta t} \leq -D_2(1-\tilde{A}V_g), \\ &V_g(t_{n+1}) \leq V_g(t_n) - D_2(1-\tilde{A}V_g)\Delta t. \end{aligned} \tag{B.3}$$

This is a recursive inequality that relates $V_g(t_{n+1})$ to $V_g(t_n)$.

Apply this iteratively over multiple time, we get:

$$V_g(t_{n+1}) \leq V_g(0) - D_2\sum_{k=1}^{n}(1-\tilde{A}V_g(t_k))\Delta t. \tag{B.4}$$

Since $\frac{dV_g}{dt} \leq 0$, it follows that $V_g(t)$ is a non-increasing function, and thus we have:

$$\begin{aligned} V_g(t_k) &\leq V_g(0), \\ 1-\tilde{A}V_g(t_k) &\geq 1-\tilde{A}V_g(0). \end{aligned}$$

Equation (B.4) becomes:

$$\begin{aligned} V_g(t_{n+1}) &\leq V_g(0) - D_2\sum_{k=1}^{n}(1-\tilde{A}V_g(0))\Delta t, \\ V_g(t_{n+1}) &\leq V_g(0) - D_2(1-\tilde{A}V_g(0))(n+1)\Delta t. \end{aligned}$$

Since $(n+1)\Delta t = t$, we get

$$V_g(t) \leq V_g(0) - D_2(1-\tilde{A}V_g(0))t. \tag{B.5}$$

Differentiating (B.5) w.r.t. t, we get

$$\frac{dV_g}{dt} \leq -D_2(1-\tilde{A}V_g(0)).$$

Acknowledgments

The authors would like to thank the anonymous reviewers for their insightful feedback and suggestions, which have significantly improved the quality of this work.

The first author sincerely thanks the University Grants Commission (UGC) for awarding the Junior Research Fellowship, whose financial support was instrumental in completing this work.

References

1. CHANDRASEKHAR, *Hydrodynamic and Hydromagnetic Stability*, Dover, New York, 1981.
2. D.D. JOSEPH, *Fluid Dynamics of Viscoelastic Liquids*, Springer Science & Business Media, New York, 2013.
3. B. STRAUGHAN, *Continuous dependence and convergence for a Kelvin–Voigt fluid of order one*, Annali dell'Universita di Ferrara, **68**, 49–61, 2022.
4. A.P. OSKOLKOV, *Initial-boundary value problems for equations of motion of Kelvin–Voight fluids and Oldroyd fluids*, Trudy Matematicheskogo Instituta imeni V.A. Steklova, **179**, 126–164, 1988.
5. V. ZVYAGIN, M. TURBIN, *The study of initial-boundary value problems for mathematical models of the motion of Kelvin–Voigt fluids*, Journal of Mathematical Sciences, **168**, 157–308, 2010.
6. B. STRAUGHAN, *Instability thresholds for thermal convection in a Kelvin–Voigt fluid of variable order*, Rendiconti del Circolo Matematico di Palermo Series 2, **71**, 187–206, 2022.
7. B. STRAUGHAN, *Thermosolutal convection with a Navier–Stokes–Voigt fluid*, Applied Mathematics and Optimization, **84**, 2587–2599, 2021.
8. B. STRAUGHAN, *Nonlinear stability for convection with temperature dependent viscosity in a Navier–Stokes–Voigt fluid*, The European Physical Journal Plus, **138**, 438, 2023.
9. A.J. BADDAY, A.J. HARFASH, *The effects of the Soret and slip boundary conditions on thermosolutal convection with a Navier–Stokes–Voigt fluid*, Physics of Fluids, **35**, 014101, 2023.
10. M. BASAVARAJAPPA, D. BHATTA, *Nonlinear stability analysis of Rayleigh–Bénard problem for a Navier–Stokes–Voigt fluid*, International Journal of Non-Linear Mechanics, **162**, 104712, 2024.
11. G.N. KAVITHA, B.M. SHANKAR, I.S. SHIVAKUMARA, *On the magnetohydrodynamic stability of channel flow of Navier–Stokes–Voigt fluid*, Physics of Fluids, **36**, 043105, 2024.
12. Z.A. AFLUK, A.J. HARFASH, *Instability of thermosolutal convection in a Brinkman–Darcy–Kelvin–Voigt fluid*, Journal of Porous Media, **28**, 1–19, 2025.
13. S. SHARMA, SUNIL, P. SHARMA, *Stability analysis of thermosolutal convection in a rotating Navier–Stokes–Voigt fluid*, Zeitschrift für Naturforschung A, **79**, 689–702, 2024.
14. V.K. STOKES, *Couple stresses in fluids*, Physics of Fluids, **9**, 1709–1715, 1966.

15. H.C. WENG, *Couple-stress effect on the effective viscosity of magnetic fluids*, Physics Procedia, **9**, 63–67, 2010.

16. SUNIL, R. DEVI, A. MAHAJAN, *Global stability for thermal convection in a couple-stress fluid*, International Communications in Heat and Mass Transfer, **38**, 938–942, 2011.

17. SUNIL, R. DEVI, *Global stability for thermal convection in a couple stress fluid: rigid boundaries*, Heat Transfer Research, **45**, 43–57, 2013.

18. Z.A. AFLUK, A.J. HARFASH, *Stability and instability of thermosolutal convection in a Brinkman–Darcy–Kelvin–Voigt fluid with couple stress effect*, Physics of Fluids, **36**, 034108, 2024.

19. J.R. LIN, *Linear stability analysis of rotor-bearing system: couple stress fluid model*, Computers & Structures, **79**, 801–809, 2001.

20. I.S. SHIVAKUMARA, S.B.N. KUMAR, *Linear and weakly nonlinear triple diffusive convection in a couple stress fluid layer*, International Journal of Heat and Mass Transfer, **68**, 542–553, 2014.

21. B.M. SHANKAR, I.S. SHIVAKUMARA, C.O. NG, *Stability of couple stress fluid flow through a horizontal porous layer*, Journal of Porous Media, **19**, 391–404, 2016.

22. A. MAHAJAN, R. NANDAL, *On the stability of penetrative convection in a couple-stress fluid*, International Journal of Applied and Computational Mathematics, **3**, 3745–3758, 2017.

23. S. CHOUDHARY, R. DEVI, A. MAHAJAN, SUNIL, *Stability analysis in a couple-stress fluid layer with variable viscosity heated from below: Different conducting boundaries*, Chinese Journal of Physics, **83**, 94–102, 2023.

24. A. THAKUR, S. KUMAR, R. DEVI, *The effect of rotation on ferroconvection in the presence of couple stress forces in porous medium: A nonlinear analysis*, The European Physical Journal Plus, **139**, 1–16, 2024.

25. Z.A. AFLUK, A.J. HARFASH, *Thermal convection in a Brinkman–Darcy and Kelvin–Voigt fluid of order one with coupled stresses effect*, Heat Transfer, **54**, 184–202, 2025.

26. G.P. GALDI, B. STRAUGHAN, *A nonlinear analysis of the stabilizing effect of rotation in the Bénard problem*, Proceedings of the Royal Society A, **402**, 257–283, 1985.

27. R. SHARMA, SUNIL, S. CHAND, *Thermosolutal instability of Walters' rotating fluid (Model B') in porous medium*, Archives of Mechanics, **51**, 181–191, 1999.

28. SUNIL, P.K. BHARTI, R.C. SHARMA, *On Bénard convection in a porous medium in the presence of throughflow and rotation in hydromagnetics*, Archives of Mechanics, **55**, 257–274, 2003.

29. M. MALASHETTY, M. SWAMY, W. SIDRAM, *Thermal convection in a rotating viscoelastic fluid saturated porous layer*, International Journal of Heat and Mass Transer, **53**, 5747–5756, 2010.

30. A. THAKUR, SUNIL, R. DEVI, *The effect of couple stresses on stability analysis of magnetized ferrofluid saturating a porous medium heated from below*, Journal of Porous Media, **27**, 85–106, 2024.

31. B. STRAUGHAN, *The Energy Method, Stability, and Nonlinear Convection*, Springer, New York, 2004.

32. A. Thakur, S. Kumar, R. Devi, *A nonlinear stability analysis for magnetized ferrofluid heated from below in the presence of couple stresses for combination of different bounding surfaces*, Numerical Heat Transfer, Part B: Fundamentals, **86**, 1, 106–122, 2023.

Received December 11, 2024; revised version March 17, 2025.
Published online May 19, 2025.